MSc. Climate Physics

Institute for Marine and Atmospheric Research Utrecht

Intraseasonal atmospheric variability under different climate trends

Universiteit Utrecht

14/12/2023

Author
Bernardo Maraldi
Student ID
1611194

Supervisor
Prof. Michael Ghil
Prof. Henk Dijkstra

E se all'improvviso una tarma si ferma sul bordo di una matita e palpita come un fuoco, guardala, io la sto guardando, sto palpando il suo piccolissimo cuore, e la sento, questa tarma risuona nella pasta di cristallo congelato, non tutto è perduto.
(Julio Cortázar)

Acknowledgments

I wish to acknowledge here the rich and insightful guidance of Michael Ghil for this master thesis. The challenges and opportunities encountered during the months spent working together in Paris have been inspiring, while enduring the conclusion of the Master's experience. I am grateful for this and for the chance of participating in the Dynamic Days Europe in Naples. It is also a pleasure to acknowledge the supervision of Henk Dijkstra and his stimulating comments in the making of this project. I want to further thank Fabio D'Andrea, for giving me the chance of discovering the ENS of Paris and for his great helpfulness, not granted.

Abstract

Low order climate models can play an important role in understanding low frequency variability in the atmospheric circulation and how it can be affected by trends in the forcing consistent with climate change. A conceptual model of the midlatitudes zonally symmetric atmospheric circulation in geostrophic equilibrium is studied from the perspective of dynamical systems theory. The model was first introduced by Lorenz in 1984. A study of the steady states and a bifurcation analysis are carried out in order to identify intervals of different behaviours in the parameter space. In the first place, the focus is put on the study of the nonautonomous system where the cross latitudinal heat contrast varies seasonally, accordingly to changes in insolation. The snapshot attractor of the nonautonomous system seasonally forced is compared with the attractor of the autonomous one for two distinct moments of the year (summer and winter). In both cases the effects of the time dependent forcing are reflected in a clear change of shape of the attractor. Predictability is lost in both cases: the summer attractor loses its periodicity when the forcing is seasonal. The winter one favours energy transport through one of the two wave components included in the model. In addition, the forcing is subjected to climate trends (both positive and negative). The analysis of the snapshot attractor of the system under climate trends suggests that the model does not follow the geostrophic assumption in certain ranges of the forcing as the average wind flow does not always show a positive dependence on the equator to pole heat contrast. On the other hand, the energy transported by the eddies follows the sign of the climatic trend. Overall, different effects are observed. A chaotic behaviour can be completely suppressed in favour of a regular periodic one and vice-versa. At the same time, circulation patterns can change, suddenly disappear and rebuild. In general, the use of the snapshot attractor proved to be a robust tool to study the internal variability of the climate as well as the changing arising from climate trends. Present and future perspectives on this work also include a spectral analysis to extensively understand the effects of climate trends on low frequency variability.

1 Introduction and Motivation

In 1984 Edward Lorenz introduced for the first time a conceptual model of the midlatitude atmospheric circulation to investigate the irregularity of the atmosphere and to study the effects of external asymmetries on an idealised Hadley cell (Lorenz, 1984 [1]). Far from being a detailed and exact representation of the real atmosphere, the model had served to study and to test existing theories about the general behaviour of the atmospheric circulation and to build new ones. In 1984, Lorenz analysed the autonomous case of the low order model and characterised it by imposing a perpetual season (either summer or winter) on the forcing acting on the system: certain values of the parameters led to intransitive periodic solutions while others induced a chaotic behaviour of the system, unveiling the existence of a strange attractor.

Given the conceptual simplification of the extra-tropical atmospheric circulation, the model (which I will refer to as L84 from now on) plays a metaphoric role. Nevertheless, dynamical system tools, when applied to such low order models, prove to be helpful both in characterizing them from a merely mathematical perspective and in drawing a general insight and understanding of the processes they capture.

Since the publication of the original paper, the L84 model has been largely studied in literature. A subsequent early work from Lorenz himself (Lorenz, 1990 [2]) revived the L84 model to study the implications of chaos on intransitivity related to the atmospheric circulation. The nonautonomous

version of the model was taken into account for the first time. These two works from Lorenz highlighted how the importance of the study of dynamical systems exceeds the boundaries of mathematics and strengthened its interdisciplinary link with physics: Lorenz used the model as a mathematical tool to test his speculative reasoning concerning the presence or absence of intransitivity in the atmosphere while characterizing the fractal structures of the strange attractor and its basin of attraction.

Further extensive work by others, concerning the study of the bifurcations, the stability and the predictability of the model was accomplished in the following years (Shilnikov et al., 1995 [3]; Broer et al., 2002 [4]; Freire et al., 2008 [5]). Researching these properties to characterize the L84 model behaviour proved to be surprisingly interesting for its applications (for the study of the atmospheric circulation only and more). On one hand, the L84 model has been used while coupled to a low order box model for the ocean (van Veen, 2001 [6]) to study the different feedbacks of the atmosphere-ocean system (where the atmosphere acts on a fast time scale and the ocean on a slow one).

On the other hand, additional fascinating purposes to study the L84 model exist: for example, a study about modelling cereal crops cycles in semiarid regions (Mangiarotti et al., 2012 [7]) advocates for further investigation and connotation of the strange attractor of the chaotic L84 version. It was found that the toroidal structure of the attractor of the L84 model shares some similarities with the attractor of their global model for normalized differential vegetation index. Beside yielding observations of geometrical similarities, the study of the L84 model could help understanding if such rich dynamics can be captured by other types of global models as well.

Therefore, the reasons to study the L84 model are diverse and several. Each of them focuses on a different perspective of the problem. The dynamical properties of the system are quite well understood as far as the autonomous case is concerned. Although major attention has been placed on the nonautonomous case too over the years, it is still interesting to research the additional information one could draw from the time dependent case, as well as it is crucial to investigate the physical processes that hide behind the mathematical equations of the system.

Section 2 describes the L84 model from a dynamical system perspective, touching upon the autonomous case and focusing on the nonautonomous one. It is introduced why the L84 model is a very suitable system to study low frequency variability in climate, such as the sub-seasonal to seasonal variability (S2S), also referred to as intraseasonal variability.

Speculations about the model counterpart in the real climate have already been tackled and remarked by Lorenz at the end of the last century. Here, the spotlight is placed on the study of the seasonal effects on the S2S variability by using dynamical systems tools such as bifurcation analysis (Section 3) and concepts, the most important and helpful of which is the snapshot attractor or pullback attractor (Section 4). The concept of the pullback attractor for nonautonomous dynamical systems is extensively covered in the work of Ghil and his collaborators (Ghil et al., 2008 [8]).

In addition to the seasonal forcing arising from changes in insolation, the main purpose of this work is to subject the L84 model to different climate trends that may resemble the effects of global warming and to study the effects on the circulation and waves patterns. As simple as it is, the system represents an idealised version of the mid-latitude atmospheric circulation whose main driver (the equator to pole heat con-

trast or temperature gradient) will very likely be affected by climate change. The westerly flows that characterise the latitude range between 30° and 60° (both north and south of the equator) are predicted to be altered by a trend in the cross latitudinal temperature gradient (expected with climate change). Nevertheless, different effects are observed and forecast at different altitudes in the atmosphere (Stendel at al., 2021 [9]): the Arctic amplification would lead to a reduction of the temperature gradient, although it can be considered to be quite a shallow phenomenon (concerning only the first few kilometers of the troposphere). Thus, the change would only affect the near-surface meridional temperature gradient. On the other hand, a higher warming and energy release in the form of latent heat is expected around the tropopause at the tropics, leading to the opposite behaviour for the meridional temperature gradient [9]. The latter case would specifically affect the extra-tropical jets (upper troposphere westerly winds) rather than the surface westerlies. Keeping in mind these considerations and the conceptual nature of the model, both scenarios (increasing and decreasing cross-latitudinal heat contrast) are taken into account. For each different scenario (seasonal forcing only and two different climate trends) the pullback attractor has been computed, here referred to also as snapshot attractor. The concept of the snapshot attractor relies on the fact that the measurements happen in a present time state, where the forcing has a specific value. It is interesting then to compare the snapshot attractor of the nonautonomous system with the forward attractor where the forcing was held fixed to the same forcing value for entire run (autonomous case) to explore the effects of the time dependence on the system.

Lastly, a summary of the main results and the final remarks are drawn in Section 5 which also touches upon future work that takes the topics presented here one step further.

2 The L84 model and seasonal effects

In the second half of the 20$^{\text{th}}$ century Edward Lorenz's work helped tracing the evolution of our understanding of the general circulation of the atmosphere (Lorenz, 1967 [10]; Lorenz, 1991 [11]). In particular, he proposed a 3-equations system that conceptually represents the mid-latitude atmospheric circulation, as an idealised atmosphere in thermal wind balance[1]. The model follows as:

$$\frac{dX}{dt} = -Y^2 - Z^2 - aX + aF, \tag{1a}$$

$$\frac{dY}{dt} = XY - bXZ - Y + G, \tag{1b}$$

$$\frac{dZ}{dt} = bXY + XZ - Z. \tag{1c}$$

The independent variables are X, Y and Z. X represents the intensity of the zonally symmetric globe-encircling westerly wind current (the westerlies). The intensity of the current is assumed to be in permanent equilibrium with the equator-to-pole temperature gradient, which is equivalent to assuming geostrophic equilibrium for the atmosphere. Y and Z represent the cosine and sine phases of a chain of superposed large-scale eddies (or waves), which are a crucial mean of poleward heat transport. In the model, the transport happens at a rate proportional to the square of the amplitudes of these waves.

All the variables are scaled so that the time unit is 5 days, roughly the time scale for

[1]Since the low dimensional L84 model does not take into account multiple atmospheric layers it would be more rigorous to talk about geostrophic balance.

the eddies to damp. Therefore, by tuning the parameter a it is possible to determine whether the westerlies damp more or less rapidly than the eddies. b is a parameter that defines the time-scale of displacement of the eddies due to the current, while F and G are external forcing terms, namely the cross-latitude external heating contrast and the asymmetric forcing arising from land-ocean heating contrast respectively.

In the model, it is the thermal forcing F that acts to change the equator-to-pole temperature gradient X. When F is kept constant and does not depend on time, the system is defined as "autonomous". In the autonomous case, traditionally, the condition $F = 8$ coincides with a perpetual winter season while the case when $F = 6$ is identified with a perpetual summer. In fact, the meridional temperature gradient varies accordingly to the interchange of seasons: it is higher during the winter and lower in the summer (because of differences in insolation). Therefore, one can consider its explicit dependence on the time to study seasonal and climatological effects. When F explicitly depends on the time t, the system is defined as nonautonomous. In the nonautonomous case where the system is seasonally forced, the forcing term appears as:

$$F(t) = F_0 + A\ cos(\omega t),\ \omega = \frac{2\pi}{\tau} \qquad (2)$$

where τ is the one year period (with $\tau = 73$ since it is the number of units of five days contained in one year). A is the amplitude of the oscillation (fixed to $A = 2$).

One can notice that no thermal inertia has been taken into account and the solar heating is the direct source of energy (as the maxima and the minima of the forcing respectively occur at the beginning and at the half of the year). The assumption here is that the principal heating comes directly from the insolation, while for the real atmosphere the underlying ocean and land are the main source (and a lag exists between the solstices and the maxima of heat provided by land and oceans).

When a global climate trend is taken into account, the constant term F_0 becomes time dependent and the forcing shall undergo a general linear decrease (if the focus is on the flow near the surface where a moderate westerly current exists) or increase (at higher altitudes where the jet-streams develop, with higher wind velocities) [9]. Specifically, in this case $F_0(t)$ assumes the following form:

$$F_0(t) = \begin{cases} \bar{F}_0,\ t < 10; \\ \bar{F}_0 \pm \alpha \dfrac{(t-10)}{T},\ t > 10. \end{cases} \qquad (3)$$

The slope of the linear trend is $\alpha = 2$, so that after $T = 100$ years have passed after the beginning of the trend, F_0 will have decreased or increased of 2 units. At $t = 0$ the starting value is $\bar{F}_0 = 7$. The value of the slope was chosen to be high enough to guarantee that the forcing would assume values consistent with different types of behaviour. In the expression (3) a 10 years time span is left for the system to reach a stationary climate. Although one could argue that a longer interval should be retained for the pre-climate change period, Drotos et al. (2015) [12] have shown that the convergence time on the attractor of the L84 model is of roughly 5 years. Therefore, during the integration, it is required that the ensemble of trajectories converges on the attractor.

For the sake of completeness, one could consider additional types of forcing that also change seasonally. For instance, G, who depicts the heat contrast between land and ocean, could also be time dependent, but throughout this work its value has always been fixed to $G = 1$. The other parameters are also kept fixed to their traditional values: $a = 0.25$, $b = 4$. The only exception takes place in section 3 where the dependence of system on a is investigated

(although a is never time dependent).
It is interesting to notice that the model can actually be derived from a truncation of a higher order model (a 2 layer model with a quasigeostrophic approximation of the midlatitudes atmospheric circulation). Van Veen (2003) [13] has shown how considerations concerning the Kaplan-Yorke dimension of the attractor suggest the existence of a globally attracting three dimensional model that the original one can be reduced to: the L84 model. In addition, even after the truncation, a detailed comparison between the bifurcation diagrams of the original model and the L84 one suggests that the 3 dimensional version (L84) still provides a good qualitative representation of the underlying phenomenon it synthesizes, such as the interaction between westerlies (jets) and the superimposed baroclinic waves or eddies.

The convenience of reducing the complex model to the three equations L84 lies in the fact that such simpler systems can be more easily numerically integrated and a more straightforward analytical study can be performed. Keeping in mind the time scaling of the variables, numerical simulations can be carried out to explore the behaviour of the model over time. Specifically, a fourth order Runge-Kutta numerical scheme with $\Delta t = 0.025$ (3 hours) has been used to integrate the system.
As a final remark of this section, a timeseries of the variable X over time for the nonautonomous case (with seasonal forcing) is shown in Fig. 1. The figure shows two consecutive years of a simulation of 20 years, starting from the winter solstice (the initial conditions being $\mathbf{X} = (2,\ 1,\ 0)$ where $\mathbf{X}$ is the coordinate vector in the phase space). As noted in [2] the system exhibits a bimodal behaviour during the summer season, with the flow displaying either slow oscillations with high amplitude or faster oscillation of smaller amplitude. The two types of behaviours shall be respectively regarded as between "active" and "inactive" summers. The distinction is made according to the amplitude of the oscillations during that season. It is interesting to relate this phenomenon to the behaviour of the waves and the total energy of the system, defined as $E_{TOT} = 0.5(X^2 + Y^2 + Z^2)$. Fig. 2 shows the energy of the system over the same time interval. One notices that during the active summer the energy of the system undergoes higher amplitude oscillations than in the inactive one, similarly to what happens to the winds. This means that during the active summer, the interaction of the flow with the waves is stronger and waves are constantly pumping and extracting higher quantities of energy from the flow. During the inactive summers there is little energy in the system and interaction between waves and the flow is much faster, leading to smaller oscillations with higher frequency (almost doubling the number of oscillations with respect to the active summer). Therefore, it is possible to look at the amplitude of the flow's fluctuations as an index of the eddy activity.
Additionally, it is important to highlight that the timeseries of X shows oscillations with a period of roughly 20 to 30 days, although the behaviour is chaotic (especially during the winter). This is true also for the inactive summer (without considering the double/triple oscillatory events), although it is less observable empirically. The frequency of such oscillations suggests that the L84 (within certain ranges of the parameters) could be a suitable candidate to investigate Intraseasonal or Sub-seasonal to Seasonal (S2S) climate variability and its changes due to climate change. This type of variability is generally associated with frequencies that span a range from few weeks to months, typically extended up to 100 days (although different definitions have been given in literature) (Vitart et al., 2019

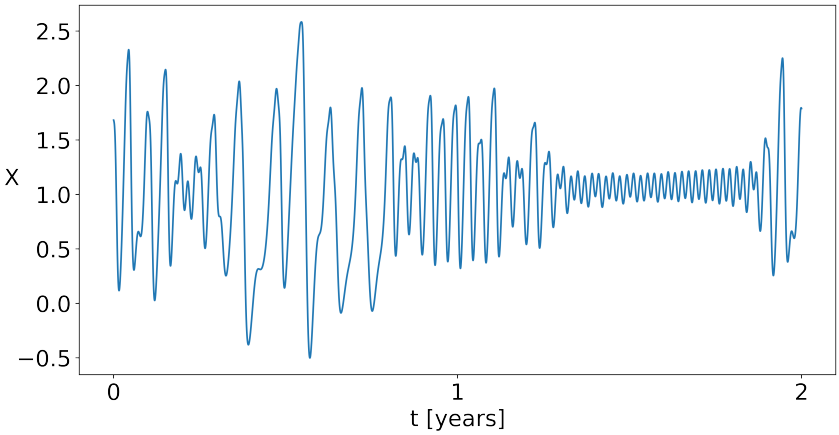

Figure 1: Final 2 years of a 20 years simulation with seasonal forcing: $F(t) = F_0 + A\ cos(\omega t)$, $\omega = \frac{2\pi}{\tau}$. Such conditions are chosen in order to achieve discontinuity between the seasons: summers are periodic and winters are chaotic. Two different behaviours arise for the summer season, which are defined *active* (first year) or *inactive* (second year). The figure seems to hint that these possible behaviours take turns over the years. At the same time, it is possible for one of the two types of summer to prevail for many consecutive years. It is the chaotic winter that randomly resets the initial conditions for the following summer and that leads to interannual variability.

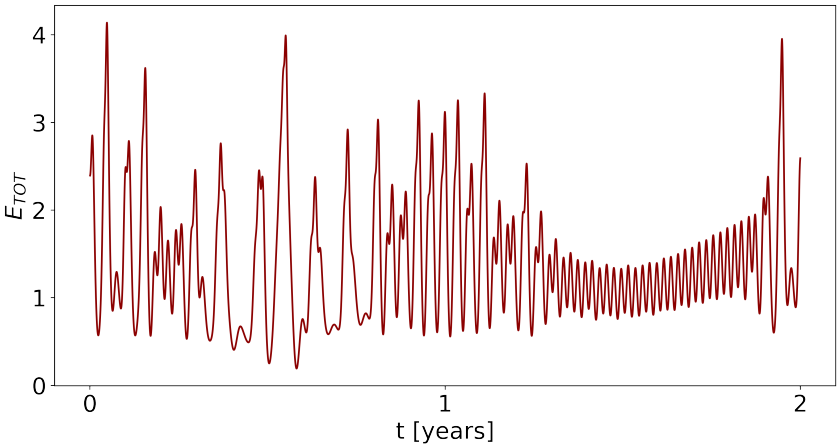

Figure 2: Energy E_{TOT} of the system over time, for the same years of 1. The active summer displays energy fluctuations with higher amplitudes and lower frequency, while the opposite happens for the inactive summer (second year).

[14]; Ghil et al., 2019 [15]). Specifically for the westerlies and extra tropical flows, the period of the variability is about 40 days, which is quite higher than what is found for the L84 model. Nevertheless, the purpose of this work it is not to provide a framework for weather or climate predictions of low frequency variability but rather to help reproducing and understanding the changes of the S2S. A more detailed spectral analysis that aims at investigating S2S variability and its evolution under climate trends can be found in the work of Maraldi B., Dijkstra H. and Ghil M..

3 System behaviour as the forcing changes

In this section the dependence of the system on the parameters a and F is researched. Specifically, analytical and numerical bifurcation analysis are carried out. The richness of the system bifurcations and predictability have been researched in papers that used more detailed softwares for the study of continuation and bifurcation problems in ordinary differential equations systems (Shilnikov et al., 1995 [3], Broer et al., 2002 [4]; van Veen, 2003 [13]). Here, the steady states of the system are studied along with two different bifurcation diagrams. The aim is to study the behaviour of the system under different values of the damping parameter a and the forcing F.

3.1 Steady states

The steady states of the system are found by setting the right hand side of equations (1a), (1b) and (1c) equal to zero. It is immediate to show that the resulting equations are:

$$Y = (1-X)G/(1-2X-(1+b^2)X^2) \quad (4a)$$

$$Z = bXG/(1-2X-(1+b^2)X^2) \quad (4b)$$

$$a(F-X)(1-2X-(1+b^2)X^2)-G^2 = 0 \quad (4c)$$

Reducing the system to the previous set of equations is also useful since ((4a)) and ((4b)) depend both on X, Y and Z while in ((4c)) the only independent variable is X. Therefore, by finding the X coordinate of the steady states it is straightforward to obtain the remaining two coordinates too. Clearly the solution depends on the free parameters, which will separately be a and F. When a is the free parameter F is kept fixed to the value $F = 6$ (but any other value would yield an analogous result). Fig. 3 hints that the system goes from 3 to only 1 real steady state as the parameter a crosses a certain threshold (which means that a subcritical pitchfork bifurcation occurs). Given the shape of the curve $f(X) = a(F-X)(1-2X-(1+b^2)X^2)-G^2$, one can analytically compute the value for which the minimum of $f(X)$ changes sign and therefore finding the critical value a_c. Computing the derivative of $f(X)$ and setting it equal to zero yields:

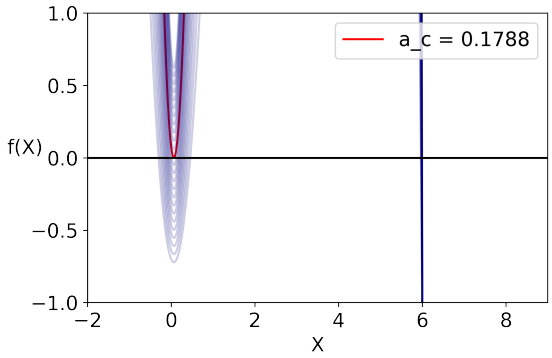

Figure 3: Graph of the polynomial $f(X) = a(F-X)(1-2X-(1+b^2)X^2)-G^2$ for different values of the control parameter a, with $F = 6$. Its interception with the y-axis coincide with the X-coordinate of the steady states of the system. When a exceeds a critical value a_c, the number of steady states changes from 3 to 1. This type of behaviour is the effect of a pitchfork bifurcation. Parameters values are $b = 4$, $G = 1$ and $F = 6$.

$$f'(X) = X^2 a(-3-3b^2) + Xa(2F+2b^2F+4) - 2aF - a = 0 \quad (5)$$

and by simplifying a from each term one finds that the solution for the minimum is $X = 0.06$. One can then manipulate the equation ((4c)) to find the relation:

$$a = \frac{G^2}{(F-X)(1-2X+(1+b^2)X^2)} \quad (6)$$

and by substituting the value of X just found, one finds that the bifurcation occurs at $a_c = 0.1788$. The value is in accordance with the behaviour found in the

bifurcation diagram reported in Fig. 4, obtained through numerical integration and presented in the following subsection. In addition to the considerations on the bifurcation, it is interesting to observe that one of the steady states is $X = 5.99$. Although this steady state is unstable, it refers to the geostrophic relation that is assumed in the construction of the model. In the original non-truncated model this is actually a thermal wind relation, as hydrostatic balance is also considered. Anyway, the steady state $X = 5.99$, for which $X \sim F$, is consistent with these approximation.
On the other hand, F can also be used as a control parameter. In this case, only the result of a numerical procedure is reported. Following the same procedure used in the previous case one will find that the system undergoes a pitchfork bifurcation for $F = 4.312$. Once again, this is in good agreement with what is found from the bifurcation diagram in Fig. 5 (see subsection 3.2).

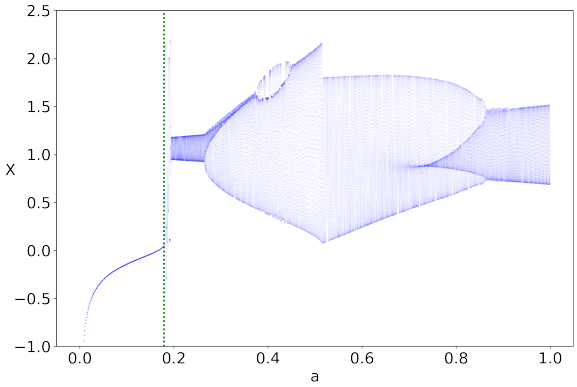

Figure 4: Bifurcation diagram of the autonomous case with a as a control parameter. a assumes 1000 different values equally spaced in the interval [0,1]. For each value of a the last 100 points of the timeseries of X are shown. The initial condition of each simulation is the final position of the previous run (except for the first one where it is set to $\{2,1,0\}$). A vertical line highlights the moment where the pitchfork bifurcation happens, in agreement with the value analitically found.

3.2 Bifurcations of the autonomous system

This section shows a bifurcation analysis of the nonautonomous system. The procedure used to build the diagram is analogous to the one used by [4]: 1000 equally spaced values of a have been selected in the parameter interval [0,1]; for F the interval is [0,10]. For each value of a and F a numerical simulation is carried out and the last 100 points of the trajectory of X in the phase space from numerical simulation are shown in Figs. 4 and 5. While the initial condition for the first value of the control parameter was $\mathbf{X}$=(2,1,0), the final position of each simulation was set to be the starting condition of the following. It is obvious that a_c defines a change in behaviour for the system, which goes from having a stable steady state to showing a periodic oscillating behaviour. When this happens one would usually expect a Hopf bifurcation to occur. In fact, a narrow band of chaotic dynamics seems to exist between the pitchfork bifurcation and the set of periodic oscillations. It is possible that the loss of stability happens in a region of the parameter space between the two.
The same procedure has been applied to study the behaviour of the system as the forcing F changes. In Fig. 5 the diagram closely resembles the one obtained for a, with the pitchfork bifurcation happening for the critical value $F_c = 4.312$. The same transition from single stable steady state to periodic oscillation through an in-between chaotic interval arises.

In addition, the parameter space has been divided in different intervals to better distinguish between areas of different behaviour and compare it with previous bifur-

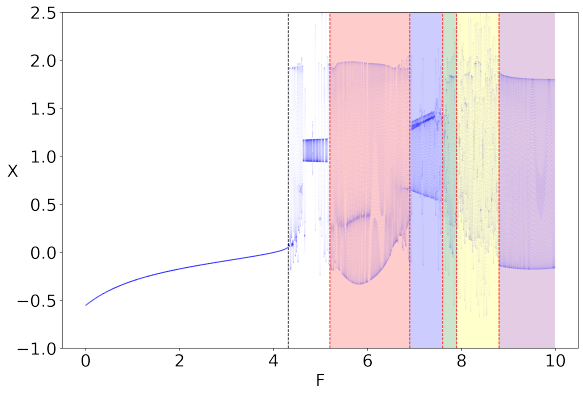

Figure 5: Bifurcation diagram of the autonomous case with F as a control parameter. F assumes 1000 different values equally spaced in the interval [0,10]. The plot is obtained following the same procedure as in 4. A black vertical line indicates where the pitchfork bifurcation occurs. The colored areas resume the distinction made by Lorenz in [2] to distinguish between different types of behaviour: intransitive periodic (red), weak periodic fluctuations (blue), weak periodic or strong chaotic (green), transitive chaotic (yellow), strong periodic (purple) behaviour.

cation analyses. Specifically, by subdividing the parameter space in the same way used by Lorenz in [2], a good agreement in terms of the type of behaviour is found. In particular, it is clear that when the parameter F assumes values in the interval [6.9, 8.8] a chaotic component appears. On the other hand, when the system evolves under a constant forcing $F < 6.9$, periodic oscillation are expected. This is in good agreement with the original choice of values of F for the summer and the winter season.

For both bifurcation diagrams one could check if a Hopf bifurcation explicitly arises in the interval between the pitchfork bifurcation. This is done through the linearization of the system around the steady state (Dijkstra, 2013 [16]). For a Hopf bifurcation to happen the theory requires the existence of a pair of pure imaginary conjugated eigenvalues for a specific value of a control parameter (Guckenheimer and Holmes, 1983 [17]) (a or F in this case), which would lead the system trajectories from reaching a steady state equilibrium to a limit cycle. This does not happen in the span between the pitchfork bifurcation and the arising of periodic oscillations (for instance, in the case of a this happens for negative values). Therefore it is presumed that the complex behaviour that arises after the critical value is exceeded is an effect of the interaction between the different solutions (steady states) already become unstable. It is interesting to notice that by looking at the imaginary part of the eigenvalues of the single steady state left for $a > a_c$ one would find the value $Im\{\lambda_{1,2}\} \simeq \pm 1.4$. From theory it is known that the imaginary part of the eigenvalue around the linearization is equal to the frequency of the oscillations in the limit cycle. In this case, the frequency of the oscillations fits in the range of frequencies found by the spectral analysis in the work of Maraldi B., Dijkstra H. and Ghil M. (about $\frac{1}{22}$ days^{-1}). Caution is needed when making this consideration which should rather act as an indicator of where the low frequency oscillations arise from in the nonautonomous case (and as additional support for the study of S2S variability). Finally, the system high sensitivity to initial conditions is highlighted for the cases where the behaviour is regular and periodic (summer season). As Lorenz had already reported in his original paper from 1984, two different trajectories starting at very close initial conditions (e.g $\mathbf{X}$={2.5,1,0} and $\mathbf{X}$={2.4,1,0}) will converge on two different limit cycles (see Fig. 6). In order to show this, a 20 years simulation with 10^4 initial conditions randomly chosen was carried out.

To conclude, the methods used here to study the bifurcation diagram might not be the most suitable to investigate it, as the

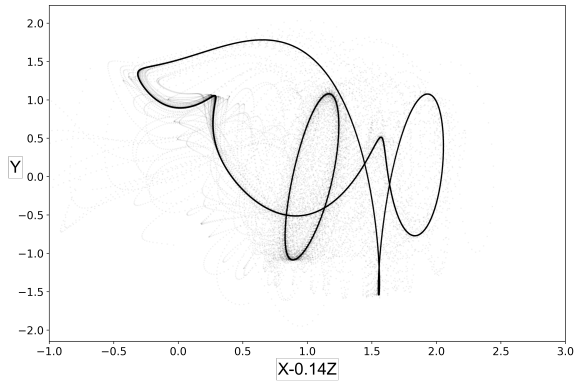

Figure 6: Projection of the attractor of a numerical simulation with 10^4 different and random initial conditions on $X - 0.14Z$. Two separate attractors can be seen when the forcing is $F = 6$. Both orbits are closed limit cycles.

initial condition of the numerical simulation used to obtain the bifurcation diagrams is just set to be the last point of the previous simulation. Nevertheless, Fig. 5 shows a good agreement in reproducing the correct type of behavior corresponding to specific regions of the parameter space used for the following analysis. For a better representation of the system behaviour dependence on the parameters a and F, one could also compute the leading Lyapunov Exponents (LEs) as a function of the control parameter. This has been partially done by Shilnikov et al. (1995) [3] and Mangiarotti et al. (2012) [7], who correctly indicate a periodic behaviour for $F = 6$ and a chaotic behaviour for $F = 8$.

4 Pullback attraction in the presence of time-dependent forcing

In the context of the study of nonautonomous dynamical systems the traditional concept of forward attraction does not work in certain cases, as the limit $t \to +\infty$ is not well defined. A new concept has to be used to replace it: the attraction is considered after the integration of a large ensemble of initial conditions that converges on the snapshot attractor [12] or pullback attractor (PBA) [18]. While this concept has been widely used in the context of random dynamical systems (Chekroun et al., 2011 [19]), a definition exists also for the case of nonautonomous deterministic dynamical systems. Detailed mathematical definitions can be found in Caraballo and Han (2016) [18] and Ghil et al. (2008) [8], respectively.

The main idea behind the concept of the PBA is the following. The key property of the PBA is that, rather than observing the asymptotic state of the system in the remote future ($t \to +\infty$), the observation occurs in a present state t, supposing that the system has evolved from an ensemble of initial conditions set at a remote initial time $t_0 \to -\infty$. In numerical practice, the initial state does not need to be asymptotically far in the past. In the physical literature, an attractor that resembles a PBA is referred to as a snapshot attractor. Here the two terms are used interchangeably. A more complete definition of a PBA is given in the Appendix.

In the case of L84, a representation of the Earth climate (where climate refers to the collection of all the possible weather configurations given by the variables X, Y and Z and following the physical laws presented in L84) is given by the so-called snapshots: they are a cross section of the PBA for a fixed time t. However, it is not really significant to talk about climate for a single instant. Thus, one should extend the concept of the climate portrayed by the attractor to a collection of the snapshots, large enough to cover a time interval where a climate can be defined (such as one month).
It is important to remark that the use of the snapshot attractor requires the initialization of an ensemble of starting conditions, rather than using only one realisation

as it was done before. In addition, Drotos et al. (2015) [12] have shown an important feature of the snapshot attractor for the seasonally forced L84 model that extends the power of the concept: while it could be intuitive to expect the attractor to be dependent on the initial conditions ensemble and the initial state it was initialised in, in reality the snapshot attractor structure shows to be independent. Any representation of the snapshot attractor at a fixed time $\bar{t}$ would look the same regardless of the initial ensemble chosen. This is true as long as time for the system to evolve is larger than the convergence time t_c, which for the L84 model is of about 5 years (Drotos et al., 2015 [12]). At the same time, the snapshot is periodic with periodic forcing. This means that, after the convergence on the attractor, any reproduction of it for a given time $t = \bar{t} + i\tau$, for i= 0, 1,...,N, with N = years, will share the same appearance. Therefore, the choice of which year to use for the attractor is arbitrary.

In order to study the PBA of the L84 model, an ensemble of 10^4 random initial conditions has been initialized in the multidimensional interval in $\mathbb{R}^3$: D defined as $D = \{(X, Y, Z) | -3 \leq X \leq 3, -3 \leq Y \leq 3, -3 \leq Z \leq 3\}$.

Every simulation is constructed with this initial conditions set, with the starting time at $t_0 = 0$. All the parameters are kept to the values that have been used before ($a = 0.25, b = 4, G = 1$). In the case where only the seasonal cycle is considered, the forcing assumes the form of equation (2), while in the case with climate trends the additional changes from equation (3) hold.

In the following subsection the focus is put on the comparison between the autonomous version of L84 and the nonautonomous one, in order to understand the sensitivity of the system to external time dependent forcing. In particular, the PBA for the nonautonomous case is compared with the forward attractor of a time independent realisation. In order to take into account the PBA, an observation time $\bar{t}$ needs to be chosen. In the case with only seasonal forcing, two different instants are considered: specifically, one where $F(\bar{t}_1) = 8$ and one where $F(\bar{t}_2) = 6$. It has already been observed that in the autonomous case, where a perpetual season is imposed, these values of the forcing correspond to a chaotic and periodic behaviour respectively. In the nonautonomous case this can not necessarily be stated only by looking at the time series, as the two types of behaviour seem to intertwine; a more detailed study must be carried out.

In addition, it is remarked that $F = 6$ and $F = 8$ are not the extrema of the forcing of equation (2). When the snapshots are computed, it would be equally reasonable to take any other time instant with different values of the forcing. Those values were chosen because they serve the purpose of not having a stationary intransitive circulation. In addition, the L84 has been largely studied when F assumes those values. Similarly, for the case when a climate trend occurs, different instants have been considered to obtain various snapshots. In this case the effect of a climate trend is reflected in a change of the shape of the attractor's structure.

Although the snapshot attractor holds in itself all the information needed to study the climate of the model, it is more practical to inspect its projection on the Y-Z plane for a comparison between different cases. The projection, which is shown as an *heatmap*, measures the number of trajectories for each possible state in that plane. In particular, the heat map is built as a bidimensional histogram extending in the interval [-3,3] on both directions, with 600 bins for each direction. An analogous analysis could be carried out by observing the Poincaré maps arising from the intersection of the trajectories with

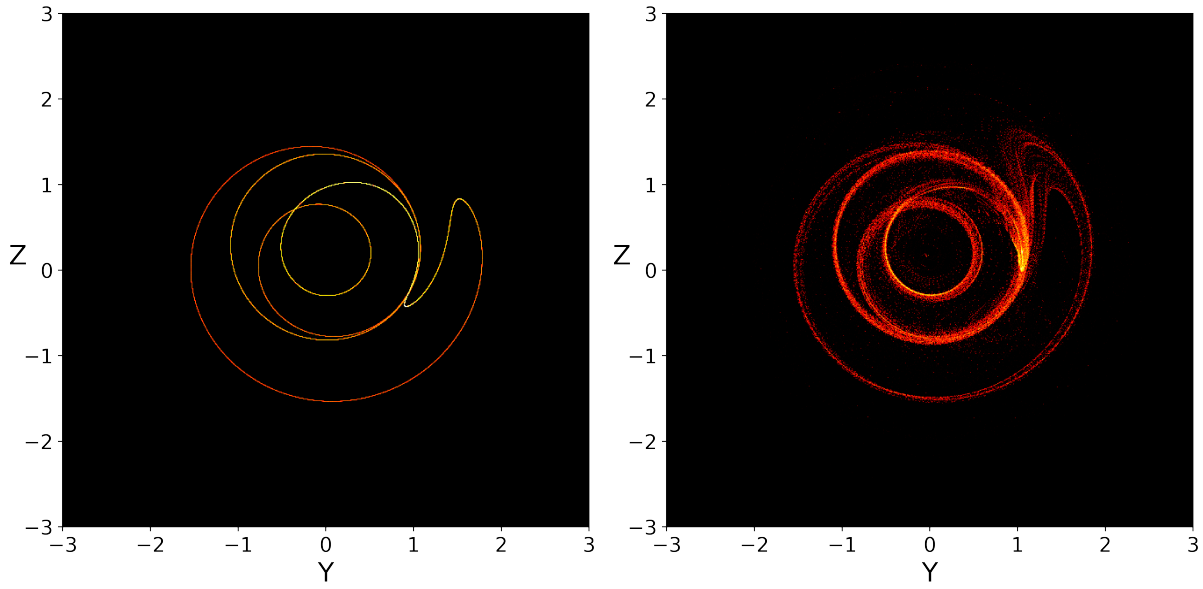

Figure 7: Heat map of the forward attractor for $F = 6$ (left) and of the snapshot attractor at the time $\bar{t}_1 = 48.6$ time units into the year, where $F(\bar{t}_1) = 6$ (right). Each of the heat maps has been made with 10^4 points which are the final state of the trajectories of the initial conditions ensemble. The initial conditions were randomly set in the interval D defined as $D = \{(X, Y, Z)| - 3 \leq X \leq 3, -3 \leq Y \leq 3, -3 \leq Z \leq 3\}$. To capture the real PBA it was necessary to let the ensemble evolve for a time larger than the convergence time of 5 years.

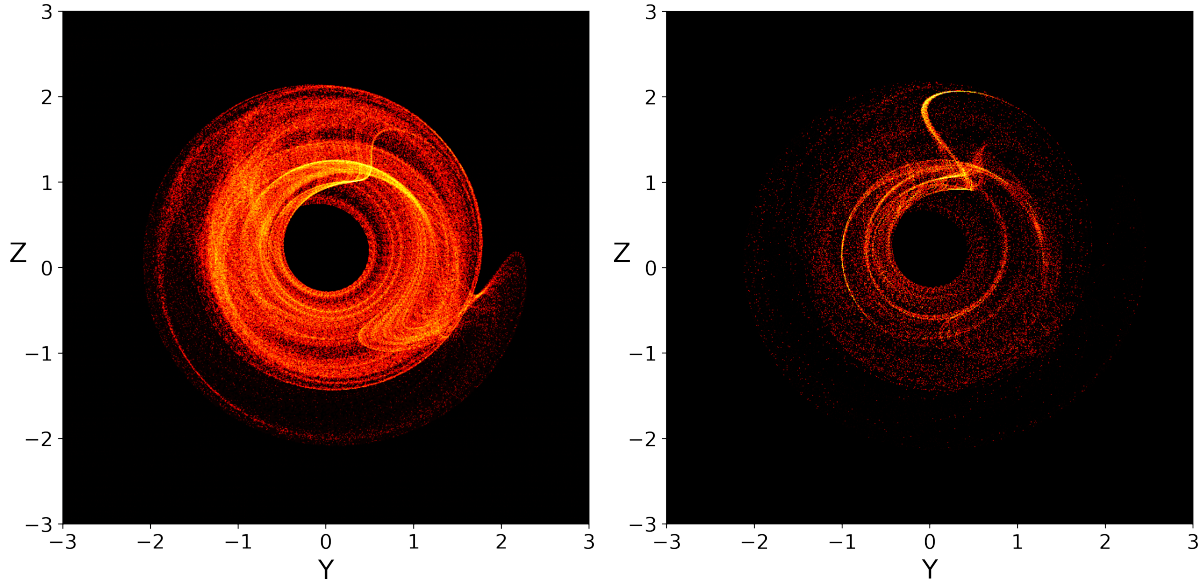

Figure 8: Heat map of the forward attractor for $F = 8$ (left) and of the snapshot attractor at the time $\bar{t}_1 = 12$ time units into the year, where $F(\bar{t}_1) = 8$ (right). The heat maps have been realised with the same procedure as in Fig. 7

an arbitrary plane in the phase space. The choice of visualizing the measure of the attractor as a heat map projection follows an example from Riechers (2022) [20]. The projection of the attractor is considered stroboscopic for the case where only seasonal forcing acts on the system, given the periodic recurrence of the same shape.

4.1 Seasonal forcing

It has been described how, for certain values of the forcing F, the system exhibits either a periodic ($F = 6$) or a chaotic behaviour ($F = 8$). When a time dependent seasonal forcing is included, this feature becomes less obvious: while, generally, it remains true for the winter season, the picture changes for the summer (Fig. 7 and 8). Nevertheless, a bimodal behaviour exists during the summer. One could suspect that this dynamic arises from the existence of two separate attractors of the system, like those shown in Fig. 6, but the mechanism seems to be more complex. In fact, during the summer of a time dependent forcing realisation, the system displays a more chaotic behaviour when compared to its autonomous counterpart (Fig. 7). This reflects the effects of the previous chaotic winter season which disrupts the existing circulation and induces less regular and periodic oscillations in the following summer (or vice-versa). In this case, periodicity and regularity seem to be lost. This means that different regions of the parameter space are visited, with less predictability and higher dependence on initial conditions. In addition, it is clear that, although a bimodal distribution exists, the slight chaotic trait of the summer attractor prevents a direct observation of low frequency variability.
In the second place, when $F = 8$ (Fig. 8), although the chaotic nature is fully conserved, there is a clear change in the shape of the attractor between the autonomous case and the nonautonomous one. On the other hand, the autonomous case shows larger uniformity in the region of the phase space explored by the system, displaying almost a symmetry between the two components of the eddies Y and Z. For the nonautonomous case, it seems that a region with significantly higher values of Z is visited by the system (the brighter fiber in Fig. 8 (b)). Keeping in mind that the attractor is a representation of the climate, this can be considered as a state with a stronger activity of one wave component (Z). Although it is bounded, the energy of the L84 model can change over time and it is not conserved. Here, the contribution of the wave component increases and extreme values are more frequently assumed.

4.2 Climatic trends

One of the aims of this project is to investigate the effects of climatic trends on the L84 model. When a seasonal forcing is applied, after about 5 years the system converges on the attractor, which can be considered the representation of a stationary climate state. In particular, the stroboscopic maps of Fig. 7 and 8 show the specific climate for a given time of the year. Clearly, some regions of the phase space where the attractor exists are explored more frequently than others by the system.
A challenging and current problem in Earth sciences is the study of the anthropogenic effects on the climate. The effects of climate change are especially difficult to investigate and to model globally due to their great regional dependence. Here, the L84 model is used to qualitatively study the effects of climatic trends in the meridional heat contrast on the mid-latitudes atmospheric circulation. Both a positive and negative linear trends are applied to the forcing F in order to capture the effect of climate change on different levels of the atmosphere. Generally, by applying a non periodical forcing to the system, one expects the attractor

to deviate from the stationary state and to change shape. The visual change of the attractors can be quantitatively remarked by observing the change in the first four moments of the distributions of the prognostic variables X, Y and Z (namely the mean, the standard deviation[2], the skewness and the kurtosis). The moments are computed about the mean.
Since it would be pretentious and pointless to investigate the changes and predict the climate for one single instant of the year, the full months of January and July are considered as references to study the effects of climate trends (one could have considered any interval long enough to have sensible depiction of a climate). This means that the attractor described in this section is a collection of the snapshots of every moment t for both months. As stated above, the forcing F follows equation (3). In order to properly capture the effects of the trend on the attractor, the year before the start of the trend is visually compared with three other different years in the interval where the trend is active (namely the 5^{th}, 50^{th} and 100^{th} year of climate change).

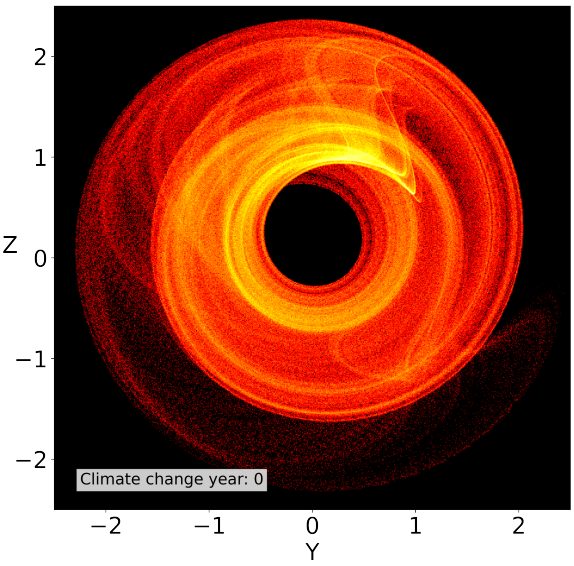

Figure 9: Projection of the attractor on the Y-Z plane for the month of January before climate change.

	Mean	Std	Skewness	Kurtosis
X	1.05	0.636	0.0164	0.336
Y	0.0102	0.905	0.0192	1.51
Z	0.421	0.981	-0.223	1.97

Table 1: Statistics for X, Y and Z in the month of January, before climate change.

4.3 Changes in the winter attractor

Firstly, the attractor of the month of January is considered. Fig. 9 shows the attractor for this month just before the start of the interval of time with the trend in the forcing.

The attractor shows a qualitative chaotic behavior (which is in accordance to the choice of the parameter range for the winter season). The distribution of trajectories on the attractor is described by the parameters in Table 1.

Fig. 12 and 13 show the changes in the attractor during the climate change period for a negative and positive trend in the forcing respectively.

When the trend is negative, the attractor does not seem to be affected by the forcing 5 years after the trend has started. On the other hand, a substantial change in the behaviour clearly arises as the system evolves further into the future. By the end of the 100^{th} year the model displays a regular behavior for the month of January. The trajectories are limited to a annulus of smaller radius (substantially reducing the range of possible combinations for the wave components Y and Z). This represents a more stable circulation where wave activity is reduced and prevented from assuming extreme values. The behaviour does not seem

[2]The strict definition of the second moment would refer to the variance of the distribution, not the standard deviation

to be periodic as the trajectories never repeat themselves but they rather fill the area within the annulus. Regardless of the weak chaotic nature of the attractor, Y and Z follow a quite circular orbit which shows how energy is equally transported by the two out of phase wave components.
The quantitative changes of the distribution of the wind flow and the eddy energy $E = Y^2 + Z^2$ for the case with a negative trend are shown in Fig. 16 (a, b), which report the dependence of the first four statistical moments on time. As far as the flow velocity is concerned, no major change in the moments is observed in the first 50 years after the climate change period has started. On average, the intensity of the wind suddenly decreases around this time, seemingly in agreement with the geostrophic equilibrium that links the equator to pole temperature gradient to the wind flow velocity. Nevertheless, the mean flow goes back to its initial value by the end of the simulation. On the other hand, the eddy energy E exhibits a decreasing trend over the entire climate change period, in agreement with the sign of the trend.
In the case where the trend is positive, by the end of year 50, the system displays a shift towards a more regular behaviour. By the end of the simulation a weak chaotic component remains, although the system seems to favour regular orbits and to approach a periodic behaviour. In chaotic systems chaos can sometimes be destroyed if a relatively strong periodic forcing acts on the system (Pikovsky, 2001 [21]), overcoming the nonlinear interaction between the variables. The result is that the forced variable starts oscillating with the same frequency as the forcing. Although the main orbits of the system analysed here have a much higher oscillation frequency than the seasonal forcing, by looking at a time series of X, Y and Z and by comparing the frequencies with $F(t)$ at the end of the simulation a pattern resembling a beat arises. In fact, the beat shares the same period as the forcing, 1 year (Fig. 10).
The average wind velocity decreases over time, while the other moments don't undergo noteworthy changes.

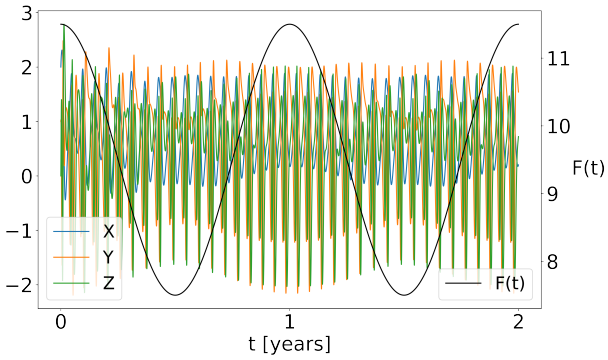

Figure 10: Timeseries of X, Y and Z for high forcing ($F_0 = 11$) and $F(t)$ over 2 years. The variables oscillates faster than $F(t)$ but they display a beat of the same frequency.

The skewness of both distributions does not exhibit considerable changes during the 100 years period and is always close to 0, indicating a symmetric distribution. This hints that energy is equally distributed between the two wave components. A relevant change is observed in the kurtosis of the distribution of E for both cases. This indicates that the distribution of eddy energy becomes light tailed. The density of outliers is reduced and less frequent extreme values of wave activity are expected.
As a final remark, the analysis on the attractor for the month of January highlights that the assumption of geostrophic balance might not hold under the range of parameter chosen, as one would expect meridional heat contrast and wind intensity to be positively correlated. This fact is not surprising given the conceptual nature of the L84 model. In addition, this could be due to the choice of parameters: Van Veen, (2003) [6] had already pointed out how the values of the parameters traditionally used in the L84 model, especially b, differ from the corre-

	Mean	Std	Skewness	Kurtosis
X	1.12	0.607	0.0106	0.340
Y	-0.0133	0.606	0.0805	0.422
Z	0.349	0.666	-0.0280	0.559

Table 2: Statistics for X, Y and Z in the month of July, before climate change

sponding physical parameters of the quasi-geostrophic two layer model the L84 can be derived from.

4.4 Changes in the summer attractor

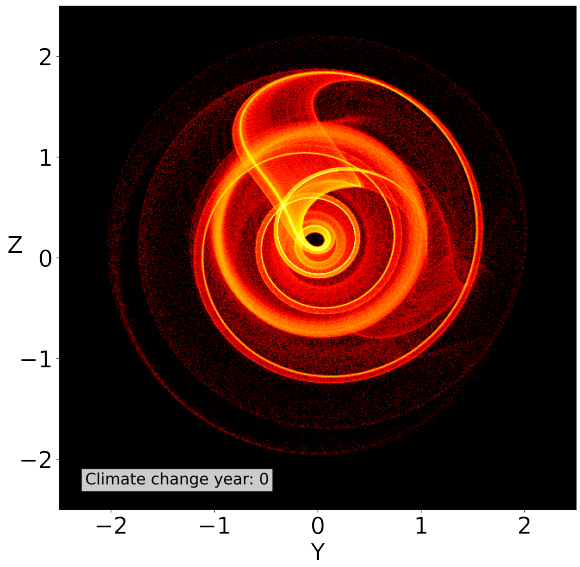

Figure 11: Projection of the attractor on the Y-Z plane for the month of July before climate change.

An analogous analysis is carried out on the summer attractor (month of July). The attractor of the system, before the linear forcing starts, exhibits a more regular behaviour compared to the winter one (although a chaotic trait is visible, as expected after the considerations of section 4.1). The statistics of the attractor of July before the climate change, shown in Fig. 11, are shown in Table 2. The case of a negative trend in the forcing is very interesting. The waves pattern seems to break down and only one soft spot is bright in the heatmap at year 50 (with $Y \sim 1$ and $|Z| < 0.5$), as shown in Fig. 14. This means that the trajectories are scattered and diffused over the phase space with respect to the other cases taken into account so far (lower density in every bin). On the other hand, a periodic pattern is observed again by the end of the simulation and the system has rebuilt a new circulation pattern. The geostrophic relation only holds until before the year 50, where the decreasing trend in the average wind velocity is disrupted. A new irregular pattern of the average wind velocity arises, while the circulation is restored by the end of the century. Overall, the average radius of the orbits in the Y-Z plane is substantially reduced and as a consequence the average eddy energy E also decreases over time. As in the winter case, when the system shifts from a chaotic behaviour to a periodic and regular one, the kurtosis of the distribution substantially decreases. As far as the case with the positive trend case is concerned, the change in behaviour highlights a loss of regularity towards chaos and unpredictability (Fig. 14). During the first 20 years of the climate change period the average wind velocity decreases and then a weak increasing trend arises. An interesting trend in the kurtosis of the energy distribution appears, with the system at first shifting from a heavy tailed distribution towards a reduction of the outliers, just to suddenly display a heavy tailed distribution by the end of the simulation. This seems to be in contrast with what happens in the previous case, where no major inversions in the statistics trend were observed. These considerations reflect the deficiencies in understanding attributing a direct relation between the thermal responses of the atmosphere to climate change and its effects on the waviness of the circulation (as far as both the amplitude and the extremes

are concerned) [9].

5 Conclusions and final remarks

In summary, the study of the three equations conceptual model of the midlatitudes atmospheric circulation introduced by Lorenz in 1984 supports the contribution of low order models to the qualitative understanding of poorly comprehended atmospheric phenomena such as low frequency variability. In the bifurcation analysis the focus has been put on the damping parameter a and on the forcing F. A similar behaviour is found for both cases: the system undergoes a subcritical pitchfork bifurcation as it passes from having three steady states to only one. Different intervals where the system alternates either periodic or chaotic behaviour are found and are in agreement with the separations found in other works ([2]). The nonautonomous system, where the cross-latitudinal forcing changes seasonally, is investigated. The differences between the climate of the autonomous system and the nonautonomous one are researched for the winter and the summer season. The time dependent forcing yields a loss of predictability for the summer season: while the forward attractor of the autonomous system consists of two different limit cycles, when the system is seasonally forced a weak chaotic behaviour arises. As far as the winter attractor is concerned, the chaotic behaviour is preserved between the two cases, but the shapes of the attractors differ: in the nonautonomous case the range of values of the wave component Y is reduced in favour of higher values of Z. The model is then forced with a cross-latitudinal heat contrast consistent with a climate change scenario. The forcing is subjected to a trend and the statistics of the system on the attractor are investigated. The system does not always follow the assumption of geostrophic balance in the range of forcing values, as a direct proportionality between X and F is sometimes missing. In fact, the westerlies are expected to weaken with a decrease of the near-surface meridional heat contrast. This is not observed for the full duration of the interval of time with a climate trend. At the same time the energy E transported by the eddies components Y and Z follows the trend of the forcing (increases for a positive one and decreases for a negative one). Since the meridional heat contrast is the source of energy for the circulation, it seems that when a trend is imposed the energy extracted from the system by the eddies also follows the change with same sign. Overall, the effects of climate change on the westerly flow that characterizes the midlatitudes is still poorly understood [9]. For instance, the direct effect of the Arctic amplification is a reduction of the near-surface meridional temperature gradient, which is usually associated with an increase of the waviness of the circulation. However, some studies (Blackport and Screen, 2020 [22]) show that simulations with persistent Arctic amplification do not exhibit an increase in wave amplitudes. On top of that, observations have also shown a missing link between Arctic amplification and waviness. To conclude, the snapshot attractor has proved to be a useful tool to investigate the statistics of the climate state, and the approach can be extended to more sophisticated models as well. At the same time, although it only serves as metaphor, the L84 model has also shown to be a useful tool in understanding low frequency variability in the atmosphere, and a further spectral analysis shall be included to better capture the effects of climate change on it.

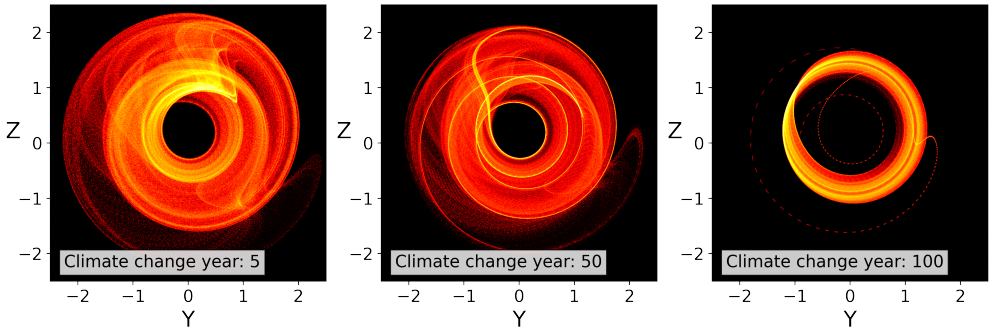

Figure 12: Projection of the attractor on the Y-Z plane for the month of January of the years 5, 50 and 100 after a negative climate trend has started.

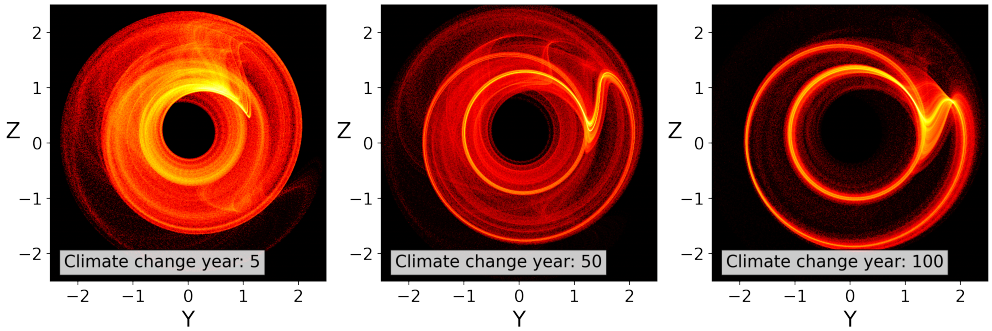

Figure 13: Same as Fig 12 but with positive trend.

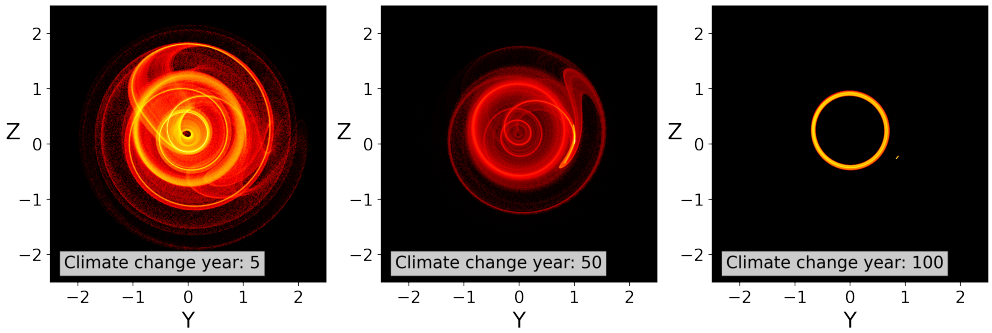

Figure 14: Projection of the attractor on the Y-Z plane for the month of July of the years 5, 50 and 100 after a negative climate trend has started.

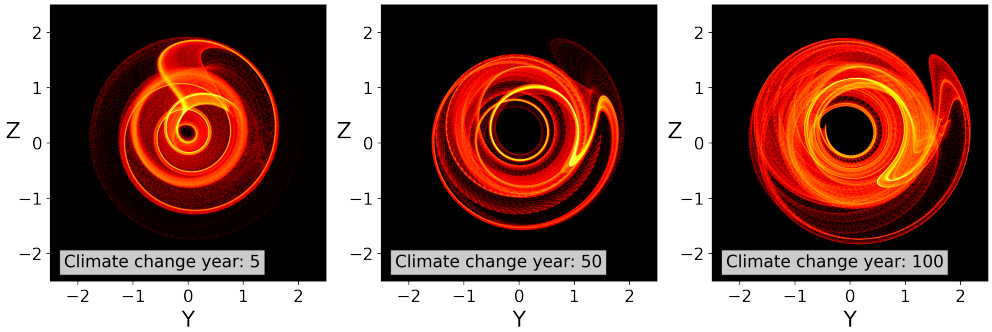

Figure 15: Same as Fig 14 but with positive trend.

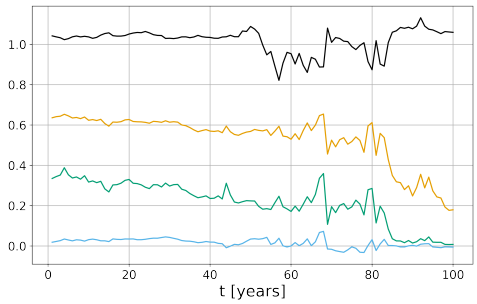

(a) Moments of X in January (negative trend).

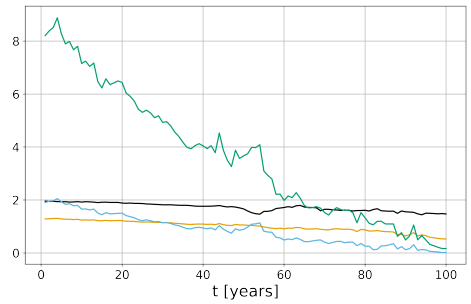

(b) Moments of E in January (negative trend).

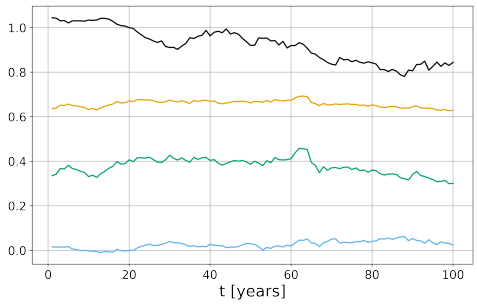

(c) Moments of X in January (positive trend).

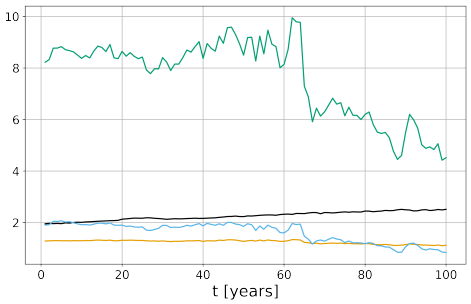

(d) Moments of E in January (positive trend).

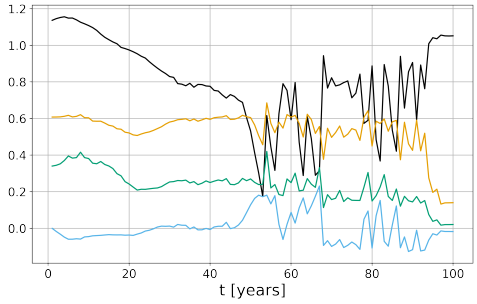

(e) Moments of X in July (negative trend).

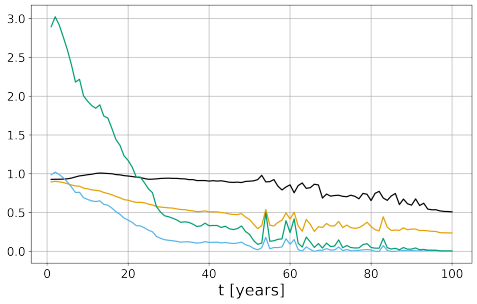

(f) Moments of E in July (negative trend).

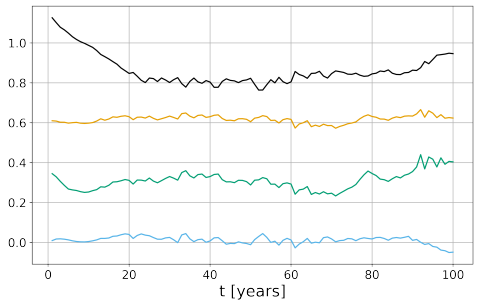

(g) Moments of X in July (positive trend).

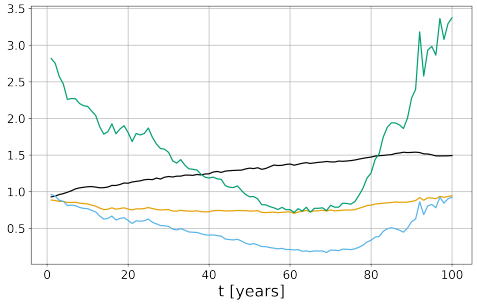

(h) Moments of E in July (positive trend).

Figure 16: Statistical moments on the attractor over time for the westerly flow X (left column) and for the eddy energy $E = Y^2 + Z^2$ (right column). Legend: black (mean), yellow (standard deviation), blue (skewness), green (kurtosis).

Appendix: Pullback attractor (PBA)

This appendix aims at providing a more detailed mathematical framework for the concept of pullback attractor in the context of nonautonomous dynamical systems. Here, the notation used by Chekroun et al. (2011) [19] and Charó et al. (2023) [23] is retained.

We consider the following system:

$$\dot{\mathbf{x}} = \mathbf{f}(t, \mathbf{x}), \tag{A1}$$

where $\mathbf{x}$ defines the state of the system in phase space and $\mathbf{f}$ determines its evolution over time. We look for the general solution $\varphi(s,t)\mathbf{x}$ of the initial value problem given by (A1) and the initial condition $\mathbf{x}(s) = \mathbf{x_0}$. For deterministic autonomous dynamical systems the operator $\varphi(s,t)$ provides only a one time description of the system, as only the interval $t' = t - s$ is of interest for the system's evolution, which is invariant with respect to translations in time. On the other hand, when the system dynamics explicitly depend on time (as described by (A1)), the solution $\varphi(s,t)$ becomes a two-parameter operator.

A new type of attraction is then defined in this case with respect to the traditional forward attraction. The result is a new object, the pullback attractor, which satisfies the following definition.

Definition: The indexed family of objects $\mathcal{A} = \{A(t)\}_{t\in\mathbb{R}}$, where each snapshot $A(t) \in \mathcal{A}$ is a compact subset of the phase space, is a pullback attractor if, for all t:

- $A(t)$ is invariant with respect to the dynamics: $\varphi(t,s)A(s) = A(t)$ for every $s \leq t$; and
- $\lim_{s\to-\infty} \mathrm{dist}(\varphi(t,s)B, A(t)) = 0$ for every bounded subset B in the phase space, where the distance is taken in the Hausdorff sense.

A forced and dissipative system for which it is immediate to show how the forward and the pullback attractions differ is the following:

$$\frac{dx}{dt} = -ax + b\sin t \ , \tag{1}$$

with the initial condition $x(s) = x_0$, where $t \geq s$. The limit for $t \to +\infty$ does not exist for any x_0. On the other hand, the limit for $s \to -\infty$ is well defined in the pullback sense above. Additional examples can be found in Chekroun et al. (2011) [19] and Riechers et al. (2022) [20].

References

[1] Edward N. Lorenz. "Irregularity: A Fundamental Property of the Atmosphere". In: *Tellus A: Dynamic Meteorology and Oceanography* 36.2 (1984), pp. 98–110. DOI: 10.3402/tellusa.v36i2.11473.

[2] Edward N. Lorenz. "Can Chaos and Intransitivity Lead to Interannual Variability?" In: *Tellus A* 42 (1990), pp. 378–389. DOI: 10.1034/j.1600-0870.1990.t01-2-00005.x.

[3] A. Shil'nikov, G. Nicolis, and C. Nicolis. "Bifurcation and Predictability Analysis of a Low-Order Atmospheric Circulation Model". In: *International Journal of Bifurcation and Chaos* 5.6 (1995), pp. 1701–1711. DOI: 10.1142/S0218127495001253.

[4] Henk Broer, Carles Simó, and Renato Vitolo. "Bifurcations and Strange Attractors in the Lorenz-84 Climate Model with Seasonal Forcing". In: *Nonlinearity* 15.4 (2002), p. 1205. DOI: 10.1088/0951-7715/15/4/312.

[5] Joana G. Freire et al. "Multistability, phase diagrams, and intransitivity in the Lorenz-84 low-order atmospheric circulation model". In: *Chaos* 18.3 (2008), p. 033121. DOI: 10.1063/1.2953589.

[6] Lennaert van Veen, Theo Opsteegh, and Ferdinand Verhulst. "Active and passive ocean regimes in a low-order climate model". In: *Tellus* 53A (2001), pp. 616–628. ISSN: 0280-6495.

[7] S. Mangiarotti et al. "Predictability of vegetation cycles over the semi-arid region of Gourma (Mali) from forecasts of AVHRR-NDVI signals". In: *Remote Sensing of Environment* 123 (2012), pp. 246–257. DOI: 10.1016/j.rse.2012.03.011.

[8] Michael Ghil, Mickaël D. Chekroun, and Eric Simonnet. "Climate dynamics and fluid mechanics: Natural variability and related uncertainties". In: *Physica D: Nonlinear Phenomena* 237.14–17 (2008), pp. 2111–2126. DOI: 10.1016/j.physd.2008.03.036.

[9] Martin Stendel et al. "The jet stream and climate change". In: *Climate Change (Third Edition): Observed Impacts on Planet Earth*. 2021, pp. 327–357. DOI: 10.1016/B978-0-12-821575-3.00015-3.

[10] Edward N. Lorenz. *The Nature and Theory of the General Circulation of the Atmosphere*. World Meteorological Organization, 1967.

[11] Edward N. Lorenz. "The general circulation of the atmosphere: an evolving problem". In: *Tellus* 43.4 (1991), pp. 8–15. DOI: 10.3402/tellusb.v43i4.15394.

[12] Gábor Drótos, Tamás Bódai, and Tamás Tél. "Probabilistic Concepts in a Changing Climate: A Snapshot Attractor Picture". In: *Journal of Climate* 28.8 (2015), pp. 3275–3288. DOI: 10.1175/JCLI-D-14-00459.1.

[13] Lennaert van Veen. "Baroclinic Flow and the Lorenz-84 Model". In: *International Journal of Bifurcation and Chaos* 13.08 (2003), pp. 2117–2139. DOI: 10.1142/S0218127403007904.

[14] Frédéric Vitart and Andrew W. Robertson. "Introduction: Why Sub-seasonal to Seasonal Prediction (S2S)?" In: *Sub-Seasonal to Seasonal Prediction: The Gap Between Weather and Climate Forecasting*. 2019, pp. 3–15. DOI: 10.1016/B978-0-12-811714-9.00001-2.

[15] Michael Ghil et al. "Extratropical Sub-seasonal to Seasonal Oscillations and Multiple Regimes: The Dynamical Systems View". In: *Sub-Seasonal to Seasonal Prediction: The Gap Between Weather and Climate Forecasting*. 2019, pp. 119–142. DOI: 10.1016/B978-0-12-811714-9.00006-1.

[16] Henk A. Dijkstra. *Nonlinear Climate Dynamics*. doi:10.1017/CBO9781139034135. Cambridge University Press, 2013. DOI: 10.1017/CBO9781139034135.

[17] J. Guckenheimer and P. Holmes. *Nonlinear Oscillations, Dynamical Systems, and Bifurcations of Vector Fields*. Springer, 1983. DOI: 10.1007/978-1-4612-1140-2.

[18] Tomás Caraballo and Xiaoying Han. *Applied Nonautonomous and Random Dynamical Systems*. SpringerBriefs in Mathematics. Springer Cham, 2016. DOI: 10.1007/978-3-319-49247-6.

[19] Mickaël D. Chekroun, Eric Simonnet, and Michael Ghil. "Stochastic climate dynamics: Random attractors and time-dependent invariant measures". In: *Physica D* 240 (2011), pp. 1685–1700. ISSN: 0167-2789. DOI: 10.1016/j.physd.2011.06.005.

[20] Keno Riechers et al. "Orbital insolation variations, intrinsic climate variability, and Quaternary glaciations". In: *Climate of the Past* 18 (2022), pp. 863–893. DOI: 10.5194/cp-18-863-2022. URL: https://doi.org/10.5194/cp-18-863-2022.

[21] Arkady Pikovsky, Michael Rosenblum, and Jürgen Kurths. *Synchronization: A Universal Concept in Nonlinear Sciences*. Cambridge Nonlinear Science Series 12. Cambridge University Press, 2001. ISBN: 9780511755743. DOI: 10.1017/CBO9780511755743.

[22] Russell Blackport and James A. Screen. "Insignificant effect of Arctic amplification on the amplitude of midlatitude atmospheric waves". In: *Science Advances* 6.8 (2020). DOI: 10.1126/sciadv.aay2880. URL: https://doi.org/10.1126/sciadv.aay2880.

[23] Gisela D. Charó, Michael Ghil, and Denisse Sciamarella. "Random templex encodes topological tipping points in noise-driven chaotic dynamics". In: *Chaos: An Interdisciplinary Journal of Nonlinear Science* 33.10 (Oct. 2023). Special Collection: Theory-informed and Data-driven Approaches to Advance Climate Sciences, p. 103141. DOI: 10.1063/5.0140660. URL: https://doi.org/10.1063/5.0140660.